Divertor heat load study in COMPASS using IR thermography and divertor probes

P. Vondracek[1,2], J. Adamek[1], J. Cavalier[1,3], A. Devitre[4], J. Horacek[1], M. Hron[1], R. Panek[1], M. Peterka[1,2], J. Seidl[1] and the EUROfusion MST1 Team[5]

[1] *Institute of Plasma Physics of the CAS, Prague, Czech Republic*

[2] *Faculty of Mathematics and Physics, Charles University, Prague, Czech Republic*

[3] *Institut Jean Lamour IJL, Université de Lorraine, Vandœuvre-lès-Nancy, France*

[4] *Universidad de Costa Rica, San José, Costa Rica*

[5] *Meyer et al., Overview of progress in European Medium Sized Tokamaks towards an integrated plasma-edge/wall solution, accepted for publication in Nuclear Fusion*

Introduction

Heat flux magnitude and distribution over first wall and plasma facing components is a key issue for next step fusion devices in order to avoid damage of inner vessel components and secure reliable operation. Radial profiles of parallel heat flux in present tokamaks and their scaling towards next step devices are thus of special interest.

Heat flux distribution in the inner and outer divertor region was studied in the COMPASS tokamak by the means of fast infrared (IR) thermography and divertor probe arrays.

Experimental setup

COMPASS tokamak is equipped with a fast IR thermography system [1] currently capable of observing either a limited radial extent of the high field side (HFS) region of the open lower divertor or full radial extent of the low field side (LFS) divertor region (figure 1). The first field of view is achieved by a direct view of the Telops FAST-IR 2K camera equipped with a standard 100 mm lens through an upper inner vertical port. A 128x4 px. large image with 0.75 mm/px. and 40-78 kHz framerate can be achieved in this setup. A special cylindrical graphite sample, 56 mm in diameter, with a flat top surface inclined 50° with respect to the horizontal plane was placed on the vertical divertor manipulator and used for the HFS heat

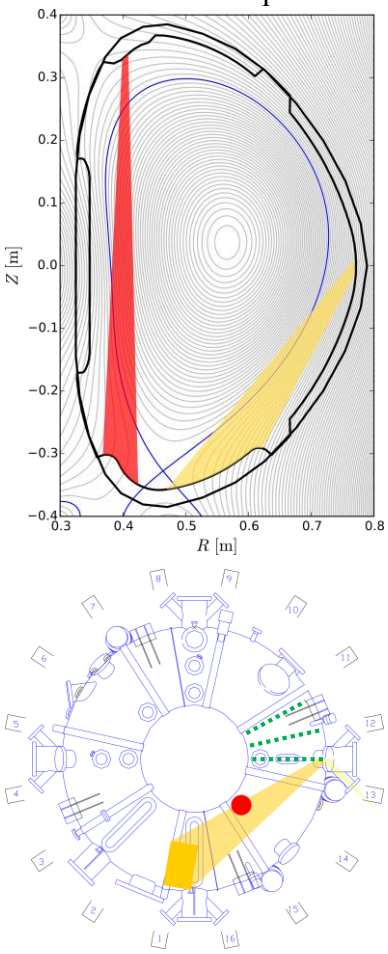

Figure 1: Experimental set-up: HFS IR view (red), LFS IR view (yellow), divertor probes (green).

flux study. High magnetic field lines incidence angles (~19°) secured high IR signal even for low integration times, necessary for fast framerates.

The second field of view is achieved by the stainless steel mirror placed in the radial outer midplane (OMP) port observed by the IR camera through the connected tangential port. An image size of 192x136 px., with a resolution of 1.5 mm/px. and a 5.6 kHz framerate is used here. Two COMPASS standard graphite divertor tiles inclined by 2° were observed on the LFS, reaching field lines incidence angles of 2 to 5°.

A recently installed set of three divertor probe arrays was used for independent heat flux profile measurements in the LFS divertor region. It provides two Langmuir probe arrays (in floating and ion saturation regime), each consisting of 53 rooftop-shaped graphite probes. The third array consists of 56 floating Ball-pen probes. The probes in each array are distributed with a 3.5 mm radial separation. Signals are acquired at a sampling frequency of 4 MHz. The combination of signals from all three arrays provides fast measurement of the parallel heat flux $q_{\parallel} = \gamma\, T_e\, j_{sat}$, where γ is the heat transmission coefficient ($\gamma = 7$ was used in this study), j_{sat} is the ion saturation current density and T_e is the electron temperature obtained from the floating Langmuir and Ball-pen probe signals as $T_e = (\Phi_{BPP} - V_{fl}) / 1.4$ (see [2] for further details).

Experimental results

Heat flux profile dependence on the plasma current I_p was studied in the LFS divertor region for ohmic L-mode discharges. All profiles were fitted by the convolution of a Gaussian and an exponential function - see (2) in [3]. Data points were mapped to the outer midplane before fitting to take into account the strong variation of poloidal flux expansion in the COMPASS open divertor (changing from approx. 15 at $R = R_{sep}$ to 6 at $R = R_{sep} + 5$ mm in a typical shot) as well as the radial variation in the heat flux absolute value mapping factor (from 1.43 to 1.33) due to changing magnetic field.

An example of the IR and probe heat flux profile for $I_p = 240$ kA is plotted in figure 2. Good agreement in the IR and probe measurements is observed, both in absolute values and profile shapes. The plasma current scan shows the

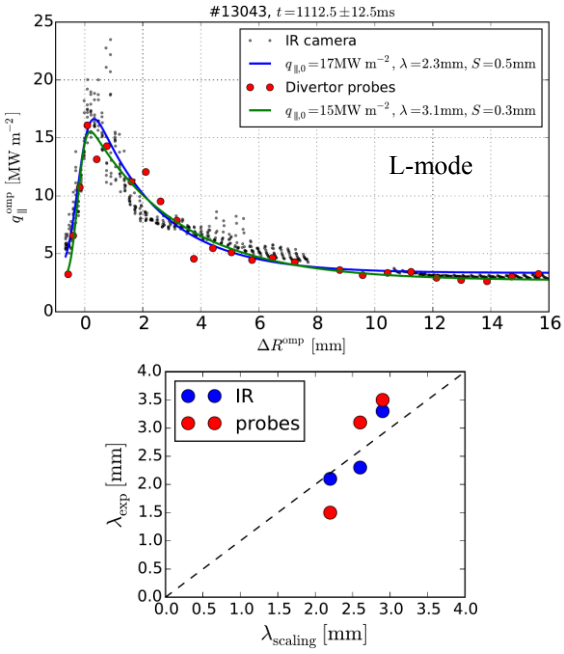

Figure 2: L-mode heat flux profile for $I_p = 230$ kA (top), λ_q comparison with scaling from AUG and JET [2].

expected behaviour of an increasing parallel heat flux at separatrix $q_{\parallel,0}$ and a decreasing heat flux decay length λ_q with increasing I_p, lying well in line with the L-mode λ_q scaling from JET and AUG $\lambda_q = 1.58 B_t^{-0.40} P_{sol}^{0.13} q_{95}^{0.73} R^{0.26}$ (mm) [4] – see bottom graph of figure 2.

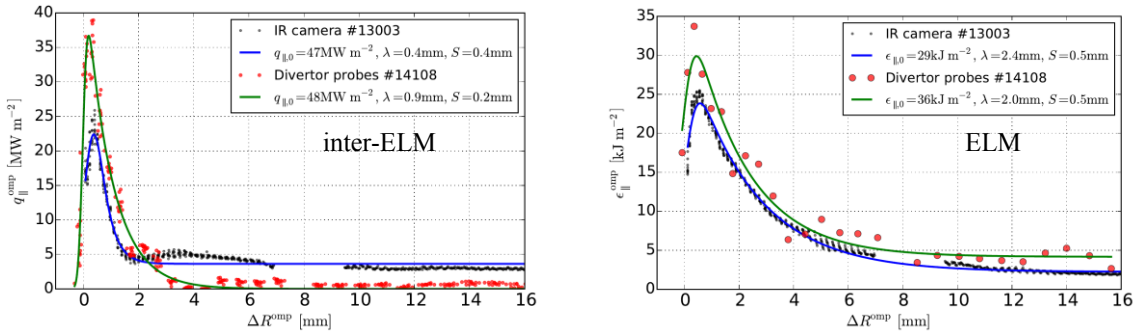

Figure 3: Inter-ELM LFS heat flux profiles (left), ELM energy density profiles (right).

In H-mode, LFS inter-ELM profiles show a steep heat flux decay close to the separatrix ($\lambda_q < 1$ mm) followed by a local minimum and a flat profile in the far scrape-off layer (SOL) - figure 3, left. Energy density profiles extracted for ELMs (time-integrated heat flux) show a much broader decay ($\lambda_q = 2.4$ mm mapped to OMP for the IR data and $\lambda_q = 2.0$ mm for probes) without the local minimum - figure 3, right. Different plasma discharges were used for each diagnostic as there is no simultaneous measurement available so far. Furthermore, the IR camera framerate below 6 kHz did not allow proper ELM peak resolution (~3 frames per ELM typically).

The HFS inter-ELM profiles have a similar behaviour (figure 4, discharge #12896). A disappearance of the local minimum was observed in a long ELM-free phase.

A difference of the inter-ELM and ELM heat flux profile was studied in the HFS divertor region. Only the region from approx. 3 to 6 mm away from the separatrix was monitored – i.e. the far-SOL profile following the local minimum in the inter-ELM profile. A simple exponential fit was used to extract λ_q because of the radially limited view. Figure 5 summarizes an example of the heat flux

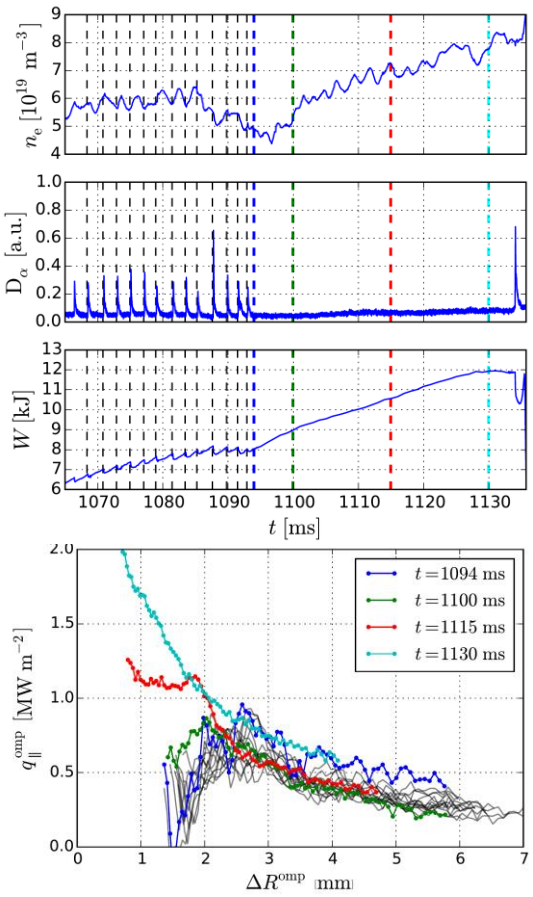

Figure 4: Bottom - Inter-ELM HFS heat flux profiles (black lines), profile evolution during ELM-free phase (color lines). Top – discharge parameters (line averaged el. density, D_α signal and plasma energy).

decay length variation during H-mode discharge #12499. Broadening of the heat flux profiles by a factor ~3 is observed for ELMs with energy around 4% of the total plasma energy in this case. However, an opposite behaviour was observed for other plasma scenarios, thus raising a necessity for a more in-detail study of this phenomena.

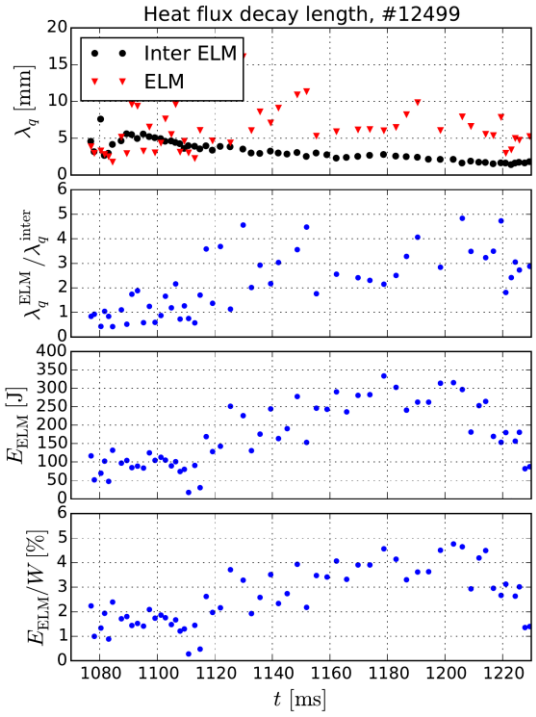

Figure 5: Heat flux decay length for inter-ELM and during ELM peak (1) and their ratio (2). Corresponding absolute (3) and relative (4) ELM size.

Conclusions

Heat flux profiles were studied in COMPASS for the first time using IR thermography. Resulting L-mode profiles are in a good agreement with divertor probe measurements and with the multi-tokamak scaling from AUG and JET showing a narrowing of λ_q with increasing plasma current.

H-mode profiles show a local minimum in the inter-ELM heat flux both in the LFS and the HFS region of COMPASS.

The variation of the heat flux profile in ELMy H-modes was studied in the far-SOL HFS divertor region showing both heat flux broadening or narrowing for different plasma scenarios. More detailed studies are thus necessary, preferentially with the new COMPASS divertor IR system planned for the end of 2017 covering the whole radial extent of the divertor.

Acknowledgement

This research has been co-funded by MEYS projects number 8D15001 and LM2015045 and Czech Science Foundation projects GA15-10723S and GA16-14228S. This work has been carried out within the framework of the EUROfusion Consortium and has received funding from the Euratom research and training programme 2014-2018 under grant agreement No 633053. The views and opinions expressed herein do not necessarily reflect those of the European Commission.

References

[1] P. Vondracek et al., *Fusion Eng. and Des.* (2017) http://dx.doi.org/10.1016/j.fusengdes.2017.05.004

[2] J. Adamek et al., *Nuclear Fusion* (2017) submitted for publication.

[3] T. Eich et al., *Journal of Nuclear Materials* 438 (2013) S72–S77.

[4] A. Scarabosio et al., *Journal of Nuclear Materials* 438 (2013) S426–S430.